Arabian Journal of Chemistry (2023) **16**, 105192

King Saud University

Arabian Journal of Chemistry

www.ksu.edu.sa
www.sciencedirect.com

ORIGINAL ARTICLE

Controlled synthesis of zinc oxide nanoparticles through flame spray pyrolysis and evaluation of their anticancer effects against gastric cancer cell

Wujun Du [a,1], Ke Feng [a,1], Cunji Li [a], Shengming Li [a], Zain Ul Abidin [b], Hua Yin [c,*], Shensi Chen [d,*]

[a] *Department of Emergency, General Hospital of Ningxia Medical University, Yinchuan, China*
[b] *Kabir Medical College, Peshawar, Pakistan*
[c] *Department of Gastroenterology, General Hospital of Ningxia Medical University, Yinchuan, China*
[d] *Department of Gastrointestinal Surgery, General Hospital of Ningxia Medical University, Yinchuan, China*

Received 13 June 2023; accepted 21 July 2023
Available online 26 July 2023

KEYWORDS

Zinc oxide;
Nanoparticle;
Flame spray pyrolysis;
Gastric cancer;
Signaling pathway

Abstract Although zinc oxide nanoparticles (ZnO NPs) have demonstrated promising anticancer activity, their therapeutic performances are frequently influenced by the synthesis routes and associated distinct physicochemical characteristics. Herein, ZnO NPs were synthesized through a cost-effective flame spray pyrolysis-assisted approach and their selective anticancer effects and underlying intrinsic apoptosis signaling pathway in human gastric carcinoma cell line (AGS) were examined. Transmission electron microscopy (TEM), Fourier-transform infrared spectroscopy (FT-IR), X-ray diffraction (XRD), and dynamic light scattering (DLS) investigations were used to characterize the synthesized ZnO NPs. Afterwards, AGS and normal fibroblast cells (L-929) were treated with various concentrations of ZnO NPs, and cell proliferation was examined by the MTT assay to determine the IC_{50} concentration of NPs. Furthermore, the quantification of ROS and apoptosis was done by fluorometer and flow cytometry assays. Additionally, superoxide dismutase (SOD) and catalase (CAT) activity assays were performed to evaluate the oxidative stress-induced cytotoxicity mediated by ZnO NPs against AGS cells. Moreover, caspase-3/-8/-9 activity and mitochondrial membrane potential (MMP) assays were done. Finally, the expression levels of p53, Bax, Bcl-2, caspase-9/-8/-3, and cytochrome *c* were assessed by quantitative real time PCR and western blot analyses to explore the probable mitochondrial apoptosis signaling pathway induced by ZnO

* Corresponding authors.
E-mail addresses: yinhua-000@163.com (H. Yin), jiaodasisi@163.com (S. Chen).
[1] These authors have contributed equally to this work and share first authorship.

Peer review under responsibility of King Saud University.

Production and hosting by Elsevier

https://doi.org/10.1016/j.arabjc.2023.105192

NPs in AGS cells. The results showed that ZnO NPs with an absorption maximum at 350 nm, an average size of 70 nm, a hydrodynamic radius of 92.89 nm, and a zeta potential of −43.13 mV potentially and selectively inhibited the proliferation of AGS cells in comparison with L-929 cells through a remarkable increase in the production of ROS, induction of apoptosis, reduction of SOD and CAT activity, activation of caspase-9/-3, and MMP disruption. Moreover, ZnO NPs triggered up-regulation of p53, Bax, caspase-9/-3, cytochrome *c* and down-regulation of Bcl-2 at mRNA and protein levels. This study suggests that synthesized ZnO NPs through flame spray pyrolysis can induce selective anticancer effects against gastric cancer cells via intrinsic apoptosis signaling pathway.

1. Introduction

Cancer is a multifactorial disease that is caused by genetic, environmental and infectious factors (Yang et al., 2020). Gastric cancer is the fourth most common cancer in the world and the second leading cause of cancer death (Yang 2006, Yang et al. 2020). Different treatments for gastric cancer are surgery, chemotherapy and radiation therapy (Orditura et al., 2014, Siddiqi and Johnston 2023). Unfortunately, chemotherapy has little effect on the treatment of gastric cancer and also high radioactive energies can partially inhibit the proliferation of cancer cells during radiation therapy (Joharatnam-Hogan et al., 2020). In most cases, radiation therapy is combined with chemotherapy and surgery for the treatment of gastric cancer (Gunderson et al., 1983, Ilson 2019). Additionally, there are drawbacks to using anticancer drugs, one of which is the development of drug-resistant cancer cells. Common cancer treatments frequently destroy healthy cells, which might harm the patient and trigger negative side effects (Debela et al., 2021). Therefore, new approaches to treating gastric cancer are required. New techniques based on nanoparticles (NPs) have been developed in order to lessen the toxic effects of anticancer drugs on normal cells and develop NPs-guided drug delivery in gastric cancer (Nagaraju et al., 2021). Recently, many NPs have been used to inhibit the progress of malignant tumor cells by reducing the systemic toxicity of anticancer drugs (Avgustinovich et al., 2021). In biomedical applications such as drug delivery and therapy, physicochemical properties of NPs plays an important role in the optimization of cancer treatment efficacy (Zein et al., 2020). In fact, in biomedical projects involving cancer, the use of NPs with a size of approximately 100 nm or less to restrict cell division and target therapeutic and diagnostic platforms has grown significantly (Avgustinovich et al., 2021). Indeed, nano-based therapeutic systems are an ideal platform for biological applications such as cancer therapy (Das et al., 2023).

Zinc oxide (ZnO) NPs have shown a great deal of attention in the treatment of cancer (Wiesmann et al., 2020). For example, it has been shown that biosynthesized ZnO NPs can show potential applications in cancer theranostics (Hameed et al., 2019). ZnO NPs have also been widely used as a potential anticancer agent *in vitro* against a wide number of cells including breast cancer cells (Shamasi et al., 2021), lung cancer cells (Rajeshkumar et al., 2018), colon cancer cells (Majeed et al., 2019), and liver cancer cells (Mohammadi Shivyari et al., 2022). Recently, it has been reported that ZnO NPs could inhibit cell proliferation through initiation of caspase-mediated apoptosis in oral cancer cells (Shanmugam et al., 2022). Additionally, it was found that ZnO NPs might reduce drug resistance in breast cancer cells while simultaneously promoting ferroptosis and controlling cell proliferation (Li et al., 2022). Therefore, ZnO NPs can be considered in the development of anticancer-assisted platforms for future trends.

Several approaches including physical, chemical, and biological methods are frequently used to synthesize NPs with different physicochemical properties (Madhumitha et al., 2016). For example, hydrothermal/microwave-mediated growth of ZnO NPs have been reported with different zinc salts for providing the source of Zn^{2+} ions (Baruah and Dutta 2009, Hasanpoor et al., 2015). However, high costs derived from the complex equipment required for hydrothermal method and lack of the reaction course monitoring of the NP growth in microwave-assisted synthesis hamper the widespread application of these methods. Among the different approaches typically used to synthesize ZnO NPs, the sol–gel way is one of the main prominent routs reported in the literature (Hasnidawani et al., 2016). However, it has been noted that the primary issues with this method are the expensive precursors and the challenging control of the reaction conditions. Another crucial strategy for the synthesis of ZnO NPs is solution combustion-assisted method, which uses the self-sustained reaction of a homogenous solution with various metal salts and natural or synthetic fuel (Ranjithkumar et al., 2021). The main shortcomings of this strategy are the requirement for ignition and the occurrence of reactions at medium–high temperatures. On the other hand, physical-associated strategies of ZnO NP synthesis are not only cost-effective but also result in radiation exposure and generation of an extensive amount of waste. Additionally, it has been demonstrated that using biologically mediated procedures produces NPs that are almost biodegradable; nevertheless, one significant disadvantage of this approach may be the inability to alter some processes (Parveen et al., 2016).

Because of its numerous advantages, such as affordability, high production rate/scale, and cost-effectiveness, manufacturing NPs using an alternative technique based on flame-based method has recently attracted a lot of interest (Trommer et al., 2010). This method was first reported by Ulrich (Ulrich 1971), where later it was used for the production of NPs in large quantities (Strobel et al., 2006). Fundamentally, the flame spray pyrolysis process works by manipulating an aqueous solution of metal ions to spray as a thin mist into a flame. Then, tiny droplets are appeared when "the solvent burns inside the flame" (Nunes et al., 2019). The pyrolysis reaction transforms the salt into metal oxide, and the metal oxide atoms are agglomerated into NPs that are subsequently collected on a substrate (Nunes et al., 2019).

Although, it has been shown that ZnO NPs may show potential anticancer effects on the gastric cancer cells, little is known about the effect of synthesized ZnO NPs through a flame spray pyrolysis-assisted approach on gastric cancer cells and possible anticancer-associated signaling pathways.

2. Materials and methods

2.1. Materials

3-(4,5-dimethylthiazol-2-yl)-2,5-diphenyl-tetrazolium (MTT), N-acetylcysteine (NAC), JC-1 (5,5′, 6,6′-tetrachloro-1,1′,3,3′-tetraethyl-imidacarbocyanine iodide), zinc acrylate (98%; CAS Number: 14643-87-9; EC Number: 238-692-3) were obtained from Sigma (St Louis, MO, USA). Fetal bovine serum (FBS), antibiotics, and cell culture media were

purchased from GIBCO-BRL (Gaithersburg, MD). All reagents and chemicals used were of analytical grade and obtained from Merck (Shanghai, China).

2.2. Synthesis of ZnO NPs through flame spray pyrolysis-assisted approach

ZnO NPs were prepared by a flame spray pyrolysis-assisted approach based on a previous report with some minor modifications (Tani et al., 2002). Briefly, zinc acrylate was used as zinc salt. A mixture of 90 vol% methanol (99.8% purity) and 10 vol% acetic acid (100% purity) was prepared and used as a solvent followed by mixing the zinc acrylate (0.5 mol/l solution) through ultrasonication. Production of ZnO NPs was performed by a spray flame reactor (Mädler et al., 2002, Tani et al., 2002). A syringe provided 5 mL/min salt solution into the oxygen-mediated atomizer (methane nozzle with a rate of 1.60 l/min and oxygen with rate of 1.55 l/min) with an oxygen flow (4.11 l/min) transferred this solution into droplets. Additionally, 10.0 l/min of oxygen was supplied to provide excess oxygen for all reactions. Finally, the produced NPs were collected by vacuum pump.

2.3. UV–visible spectroscopic analysis

The UV–visible spectroscopic assay of ZnO NPs (0.1 mg/mL, prepared in ethanol) synthesized using a flame spray pyrolysis-assisted approach was performed at room temperature with a UV–visible PerkinElmer device in the range of 200–700 nm.

2.4. Fourier-transform infrared (FT-IR) spectroscopic analysis

FT-IR spectroscopy of prepared samples with the KBr pellet method was done at room temperature employing a 1000 FT-IR instrument (Perkin-Elmer, Waltham, MA, USA) between 4000 and 400 cm^{-1} at a resolution of 10 cm^{-1} in the transmittance mode.

2.5. X-ray diffraction (XRD) analysis

Crystal structure of synthesized ZnO NPs was detected employing Smartlab X-ray powder diffractometer through Cu-Kα radiation at $\lambda = 1.5418$ Å in the $2\theta = 20$–$80°$ range and 5°/min scanning rate.

2.6. Transmission electron microscopy (TEM) analysis

Size of the synthesized ZnO NPs after preparation and air-drying at room temperature was assessed by a TEM machine [Jeol TEM model JEM-1101 (Japan)] operating at accelerating voltage of 80 kV.

2.7. Dynamic light scattering (DLS) analysis

The mean uniform particle size and surface-charge distribution of ZnO NPs derived from a flame spray pyrolysis-assisted approach (0.05 mg/mL, prepared in ethanol) were determined by DLS assay. Therefore, a Zetasizer Nano ZS (Malvern Instruments Ltd., UK) was used to assess the hydrodynamic radius and zeta potential of synthesized ZnO NPs in solution.

2.8. Cell culture

AGS (human gastric adenocarcinoma) and normal L-929 (normal fibroblast cell line) were provided by American Type Culture Collection (Rockville, MD, USA). The cells were cultured in RPMI 1640 medium supplemented with FBS (10%), penicillin–streptomycin (1%) at 37 °C and 5% CO_2.

2.9. MTT assay

MTT assay was done to explore the cytotoxic effect of different concentrations of ZnO NPs (0.01, 0.1, 1, 10, and 20 µg/mL) on AGS and L-929 cells. First, a 150 µL culture medium having 1×10^4 cells were seeded into 96-well plates for 24 h. Different concentrations of ZnO NPs were then added and incubated for additional 24 h. Afterwards, MTT solution (0.5 mg/mL) was added and incubated for 4 h followed by addition of DMSO. Finally, optical density was read employing an ELISA reader at 570 nm. The cells without any treatment were used as a negative control. The outcomes were expressed as viability percentage and IC_{50} value was determined using Graph Pad prism software using the absorbance values.

2.10. Reactive oxygen species (ROS) and apoptosis assays

Quantification of ROS in AGS cells (1×10^6 cells/ 6-well tissue culture plates) was determined using the DCFDA/H_2DCFDA-ROS assay kit (ab113851, UK). The cells were incubated with IC_{50} concentration of ZnO NPs for 4 h and then DCF intensity assay was done following incubation of cells with H_2DCFDA (20 M) for 30 min. Afterwards, DCF intensity was measured on a plate-reading fluorometer (Molecular Devices SpectraMax Paradigm Multi-Mode, Sunnyvale, CA, USA) at $\lambda_{Ex}/\lambda_{Em}$ 484/525 nm. To assess apoptosis by Annexin V-fluorescein isothiocyanate staining, AGS cells (1×10^6 cells/ 6-well tissue culture plates) incubated with and without IC_{50} concentration of ZnO NPs at 37 °C for up to 24 h, were harvested and centrifuged (1000 × g for 5 min). Afterwards, the cells were resuspended in 1 mL of binding buffer supplemented with Annexin V-fluorescein isothiocyanate (1.25 µL, 200 µg/mL) and incubated for 15 min at ambient temperature in the dark. The cells were collected (1000 × g for 5 min) and quantitated using a flow cytometry device (Biocompare, South San Francisco, CA, USA).

2.11. Superoxide dismutase (SOD) and catalase (CAT) activity assay

The biochemical assays for SOD and CAT were performed to assess the endogenous antioxidant activity in ZnO NPs treated AGS cells after 24 h. The cell suspension was prepared after treatment with IC_{50} concentration of ZnO NPs and processed for biochemical assays. Briefly, after incubation of the cells, homogenization, and centrifugation, the protein content in the supernatant was assessed by Bradford assay (Kielkopf et al., 2020). Afterwards, a determined amount of protein was used for enzyme assay based on the protocols recommended previously (Sinha 1972, Das et al., 2000).

2.12. Caspase activity assay

The caspase-3/-8/-9 activity assays were done employing colorimetric assay kits. Selective peptides were used as the substrate for caspase-3 [Caspase-3 Assay Kit (Colorimetric) (ab39401)], caspase-9 [Caspase 9 Assay Kit (Colorimetric) (ab65608)], and caspase-8 [Caspase-8 Assay Kit (Colorimetric) (ab39700)] probed with p-nitroaniline (pNA). Briefly, after treatment of AGS cells with IC_{50} concentration of ZnO NPs for 24 h, cells were homogenized and supernatants were collected. After determination of protein concentration by Bradford assay, a fixed amount of protein was incubated with the reaction buffer having dithiothreitol and substrates at 37 °C. Caspase activity assays were then done by reading the absorbance at 405 nm by a microplate reader.

2.13. Measurement of mitochondrial membrane potentials (MMPs) analysis

MMPs analysis was done using JC-1 as a potential-sensitive dye. Briefly, after treatment with IC_{50} concentration of ZnO NPs for 24 h, cells (1×10^6 cells/ 6-well tissue culture plates) were collected, incubated with JC-1 (5 μM) for 30 min at 37 °C, washed with PBS. Finally, fluorescence measurement of samples was done using a plate-reading fluorometer (Molecular Devices SpectraMax Paradigm Multi-Mode, Sunnyvale, CA, USA) and the ratio of red to green signal was assessed at λ_{Ex} = 485 nm, λ_{Em} green = 520 nm, λ_{Em} red = 590 nm).

2.14. Quantitative real time-PCR

After treatment of AGS cells (1×10^6 cells/ 6-well tissue culture plates) with IC_{50} concentration of ZnO NPs for 24 h, RNA extraction and cDNA synthesis were done in accordance with RNA Purification Kit (Thermo Fisher Scientific, USA) and Revert AidTM First Strand cDNA Synthesis Kits (Fermentas, Germany), respectively. SYBER Green method was employed to quantify the expression of mRNA, where GAPDH mRNA was used as internal control. The quantitative real time-PCR method and primers were used based on the study reported previously (Radziejewska et al., 2021) on a real-time PCR detection system (Bio-Rad, CA, USA). The relative expression of mRNA was determined and normalized using the $2^{-\Delta\Delta Ct}$ method.

2.15. Western blotting analysis

Western blotting was done to quantify the expression of proteins in AGS cells after treatment with IC_{50} concentration of ZnO NPs for 24 h based on previous reports (Li et al., 2013, Ji et al., 2015). The cells (1×10^6 cells/ 6-well tissue culture plates) were seeded, homogenized, centrifuged at 10,000 rpm for 15 min, and supernatants were used. Proteins (20 μg/lane) were loaded onto 12% SDS-PAGE, transferred to PVDF membrane, blocked by TBST solution containing 5% (w/v) non-fat milk for 2 h, incubated overnight with primary antibodies [anti-caspase-3, anti-caspase-8, anti-caspase-9, cytochrome *c,* and GAPFH (Cell Signaling Technology (Beverly, MA)), anti-Bax and anti-Bcl-2 (Santa Cruz Biotechnology (Santa Cruz, CA))], washed with TBST buffer, and finally incubated for 1 h with the secondary antibody, horseradish peroxidase-conjugated goat anti-rabbit IgG [Santa Cruz Biotechnology (Santa Cruz, CA, USA)]. The samples were detected employing a western blotting luminal reagent (Santa Cruz Biotechnology).

2.16. Statistical analysis

Data are expressed as means ± standard deviations (SD) of outcomes obtained in triplicate. Statistical analysis was done with the paired Student's *t*-test. Statistical significance was reported for $P < 0.05$. For cellular assays, control cells were used with no addition of ZnO NPs.

3. Results and discussion

3.1. Uv–visible analysis

NPs with unique electronic and optical features show quantum confinement effect. Determination of the optical characteristics of quantum size fabricated NPs can be achieved potentially with the UV–visible absorption technique (Vinayagam et al., 2022). Fig. 1a shows the absorption maximum of the synthesized ZnO NPs. A strong absorption peak (λ = 350 nm) verified the formation of ZnO NPs deduced from the surface plasmon resonance (Vinayagam et al., 2022). The movement of electrons from the valence to the conduction band may be the cause of this distinctive spectrum and band (Darvishi et al., 2019). The relevant bandgap energy (*E*) for the fabricated ZnO NPs through flame spray pyrolysis was determined as 3.54 eV, using the well know equation, E = 1240/λ, where λ denotes the wavelength of the absorption peak (λ = 350 nm). The value of *E* from the current study agrees well with the values determined previously for the synthesis of ZnO NPs using different routes, such as biological (Vinayagam et al., 2021), chemical (Kumar et al., 2013), and physical approaches (Villanueva et al., 2006).

3.2. FT-IR analysis

FT-IR spectrum of synthesized ZnO NPs was read at room temperature. FT-IR analysis is an essential assay to reveal the production of ZnO NPs, the purity of NPs, as well as the vibration of Zn—O bonds (Teimouri et al., 2018). Fig. 1b displays the FT-IR spectrum of the fabricated ZnO NPs. The peaks around 480 cm^{-1}, 940 cm^{-1}, and 3460 cm^{-1} attributed to the stretching vibration of Zn—O, stretching vibration of Zn—OH, and oscillating vibration of O—H species, respectively, which is in good agreement with previous report (Al-Nassar and Hussein 2019). In fact, a wide vibration band at 3460 cm^{-1} could be associated with O—H vibrational stretch or absorption of water molecules from the environment (Vinayagam et al., 2022). The bands observed at 480 and 940 cm^{-1} are attributed to the asymmetric Zn—O stretch, which indicated the formation of hexagonal structure (wurtzite) of ZnO NPs (Vinayagam et al., 2023). Hence, the absence of different functional moieties endorses the purity of ZnO NPs synthesized through flame spray pyrolysis.

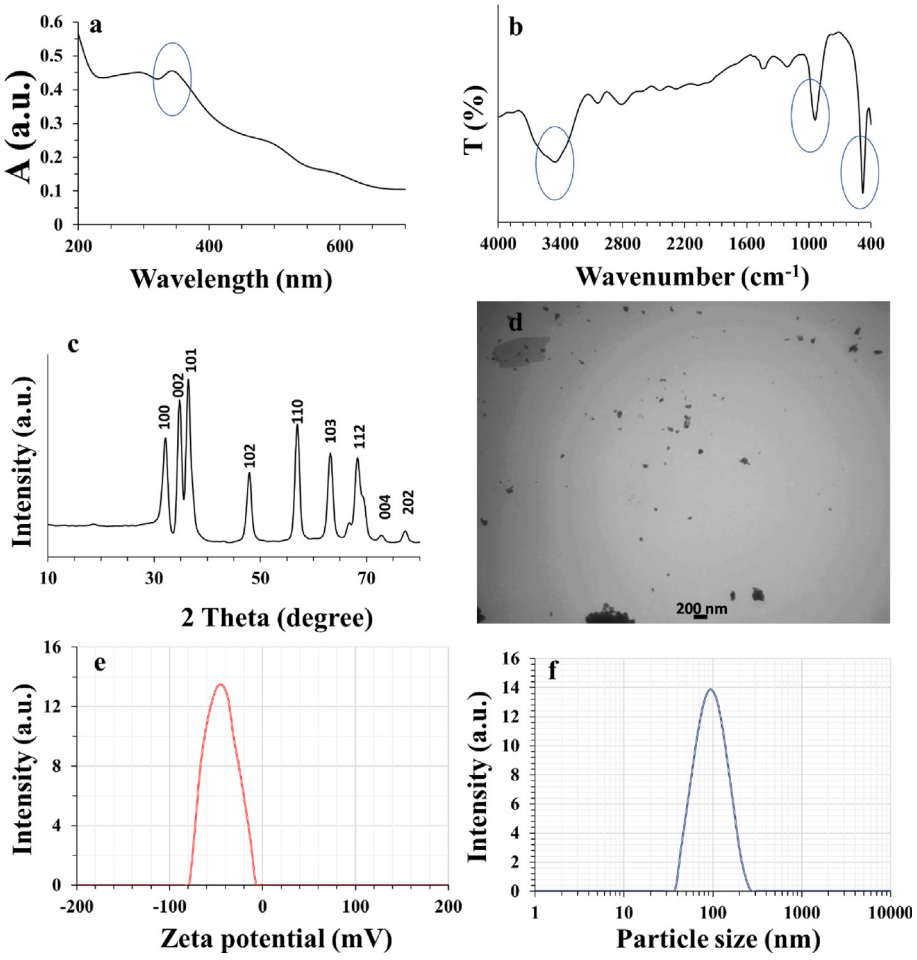

Fig. 1 Characterization of ZnO NPs. (a) UV–visible, (b) FT-IR, (c) XRD, (d) TEM, (e) zeta potential, and (f) hydrodynamic radius analyses of ZnO NPs synthesized through flame spray pyrolysis approach.

3.3. XRD analysis

XRD analysis endorsed the crystallite characteristic and phase purity of the ZnO NPs synthesized through flame spray pyrolysis. The crystallite structure of the ZnO NPs was confirmed by the nearly sharp peaks with narrow widths. In fact, the peaks at the following 2θ values (°) of 32.25°, 34.95°, 36.50°, 47.95°, 57.15°, 63.35°, 68.40°, 73.25° and 77.65° are attributed to the lattice planes of (100); (002); (101); (102); (110); (103); (112); (004); and (202), respectively (Fig. 1c), which are consistent with the standard for hexagonal structure as per JCPDS: 36–1451 (Vinayagam et al., 2022). Neither intermediates nor by-products were detected by diffraction peaks, indicating that the process yielded pure ZnO NPs.

3.4. TEM analysis

It is evident from Fig. 1d that the ZnO NPs have a sphere-shaped texture with a tendency to be aggregated. The flame spray pyrolysis led to the formation of the ZnO NPs with a moderate nucleation growth yielding the sphere-modeled morphology. Fig. 1d depicted that fabricated ZnO NPs are nearly homogeneous with an average diameter of around 70 nm.

Non-comparable results have been reported previously using many different chemical and physical routes as well as flame spray pyrolysis process for the synthesis of ZnO NPs. For example, it has been shown that ZnO NPs synthesized through a flame spray pyrolysis process with zinc nitrate as a precursor shows different diameters of around 200 nm (Carroz et al., 1980) and 10 nm (Matsoukas and Friedlander 1991), depending on the normal or spry-derided precursors. Furthermore, it was observed that the use of zinc acetylacetonate in flame aerosol synthesis approach results in the formation of ZnO NPs with a diameter of around 25–40 nm (Jensen et al., 2000). Also, it has been demonstrated that evaporation and oxidation-mediated synthesis of ZnO NPs resulted in the formation of NPs with a size of less than 30 nm with the using of zinc metals as precursor (McCARTHY et al., 1982). Therefore, it can be concluded that several parameters such as the type of synthesis route, precursors, and solvents as well as precursor solution feed rate can play a key role in the diameter of synthesized NPs and aggregation.

3.5. DLS analysis

The DLS analysis is well-known to determine the hydrodynamic size of the NPs. The average size of the ZnO NPs synthesized through flame spray pyrolysis approach was also

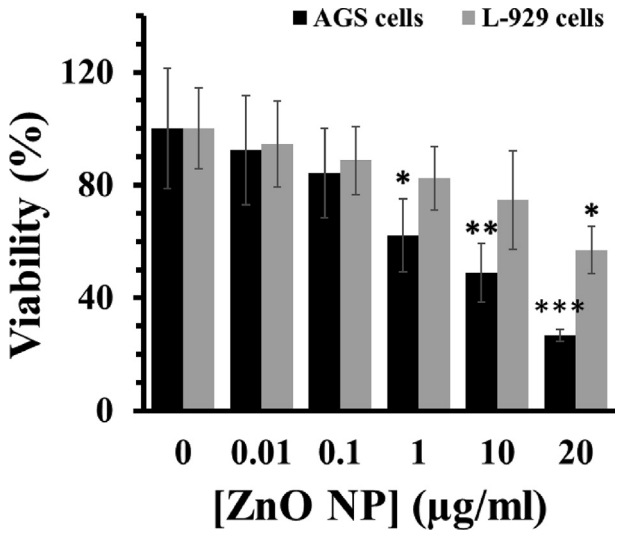

Fig. 2 Percentage cell viability due to incubation of cells with various concentrations of ZnO NPs for 24 h as assessed by MTT assay. Each data reported as the mean ± SD of three experiments. *p < 0.05, **p < 0.01, ***p < 0.001.

measured by DLS analysis. The hydrodynamic radius and zeta potential values for ZnO NPs were obtained at room temperature by DLS analysis. The zeta potential *vs.* intensity (Fig. 1e) and size distribution *vs.* intensity graphs (Fig. 1f) have been shown.

It was determined that zeta potential and the hydrodynamic radius values of synthesized ZnO NPs were −43.13 mV and 92.89 nm, respectively. These data reflect the potential fabrication of ZnO NPs through flame spray pyrolysis process. These results demonstrate potential colloidal stability and dispersion of ZnO NPs hydrodynamically. The hydrodynamic NP size was larger relative to the TEM outcome. The large size of NPs detected by DLS is associated with the event that the measured radius also includes the water molecules enveloping the core of the ZnO NPs as well as the aggregation tendency of ZnO NPs in solution (Sujitha and Kannan 2013). In fact, the large NP size could also be derived from the presence of van der Waals interaction as one of the main forces determining the colloidal stability of NPs. Also, variations in sample preparation and the magnitude of polydispersity index can have a key role in controlling the size of NPs by different techniques (Sujitha and Kannan 2013). Therefore, extensive investigations need to be done when the NP sizes are a matter of interest and the resultant data should be compared to ascertain their reactivity for selective implementations.

3.6. MTT assay

To assess the cytotoxic effect of ZnO NPs on the growth of AGS and L-929 cells, cells were treated with increasing concentrations of ZnO NPs for 24 h, and cell viability was then deter-

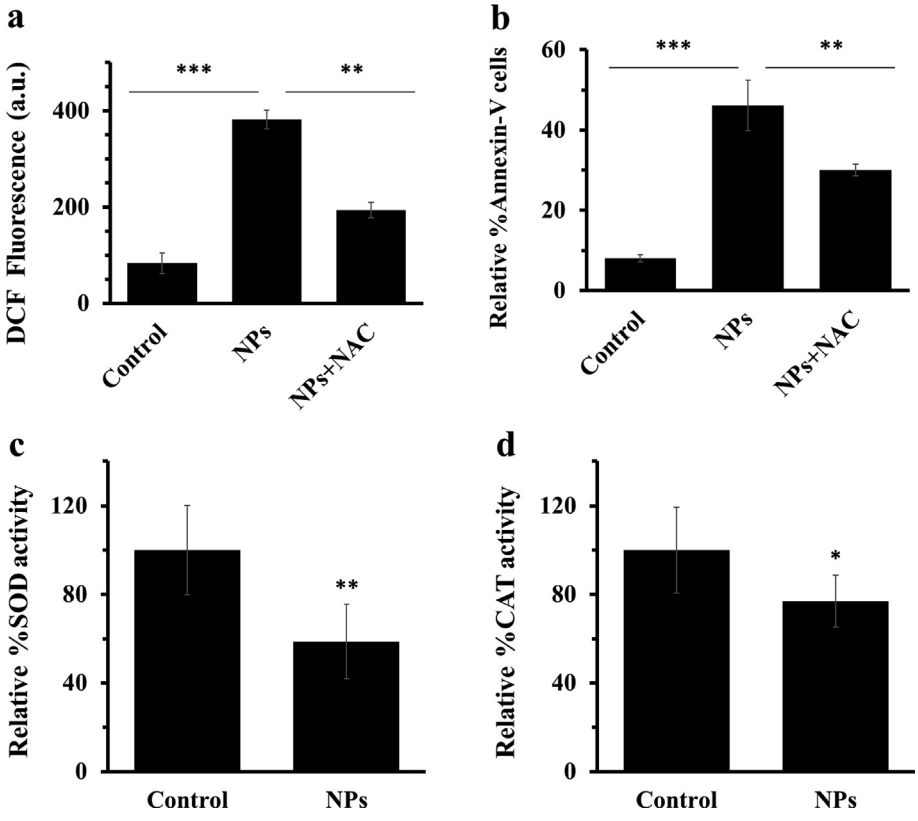

Fig. 3 (a) quantification of 2′-7′ dichlorofluorescein (DCF) intensity of AGS cells with IC_{50} concentrations of ZnO NPs after 4 h, (b) quantification of the percentage of Annexin-V FITC-positive cells, (c) percentage of SOD activity, (d) percentage of CAT activity after incubation of AGS cells with IC_{50} concentrations of ZnO NPs for 24 h. Each data reported as the mean ± SD of three experiments. *p < 0.05, **p < 0.01, ***p < 0.001.

mined with the MTT assay. As shown in Fig. 2, cell viability was concentration-dependently attenuated by ZnO NPs in AGS and L-929 cells, whereas this cytotoxic effect was more significant in the case of AGS cells. The IC_{50} determination was performed to detect the cytotoxic effect of ZnO NPs. It was seen that the IC_{50} values of ZnO NPs against AGS and L-929 cells were 8.37 ± 0.93 μg/mL and > 20 μg/mL, respectively. This data may indicate the selective anticancer effect of ZnO NPs against AGS cells.

3.7. Oxidative stress and apoptosis assays

Oxidative stress could be appointed as a primary cause of cell death mediated by NPs (Nagar et al., 2022). This phase stimulated the generation of high level of ROS and subsequent apoptosis through inactivation of antioxidant enzymes such as CAT and SOD (Alarifi et al., 2013, Alavi and Yarani 2023). In this study, it was revealed that ZnO NPs increased the generation of intracellular ROS (Fig. 3a) and induction of apoptosis (Fig. 3b) through subsequent decrease in the activity of antioxidant enzymes. Indeed, enzyme activity indicated the decreased levels of SOD (Fig. 3c) and CAT (Fig. 3d) activity after incubation of AGS cells with IC_{50} concentration of ZnO NPs for 24 h. These data showed that ZnO NPs may stimulate oxidative stress and apoptosis through inactivating CAT and SOD in AGS cells. To further explore the effect of ZnO NPs mediated by ROS on the induction of apoptosis, the cells were co-incubated with IC_{50} concentration of ZnO NPs and NAC (5 mM). It was seen that the generation of ROS and apoptosis were reduced after co-incubation of cells with ZnO NPs and NAC as a potential antioxidant (Fig. 3a, b). It has been also indicated that ZnO NPs incubation triggers apoptosis by enhancing the generation of intracellular ROS levels in LTEP-a-2 cells (Wang et al., 2015). Furthermore, ZnO NPs with a crystallite size of 21.59 ± 4.8 9 nm have been able to selectively induce apoptosis in human cancer cells through ROS production (Akhtar et al., 2012).

3.8. Caspase activity assay

Caspases are potential activators of apoptosis in both intrinsic (caspase-9) and extrinsic (caspase-8) signaling pathways (Hongmei 2012, Redza-Dutordoir and Averill-Bates 2016) which can be initiated by excessive content of ROS. As demon-

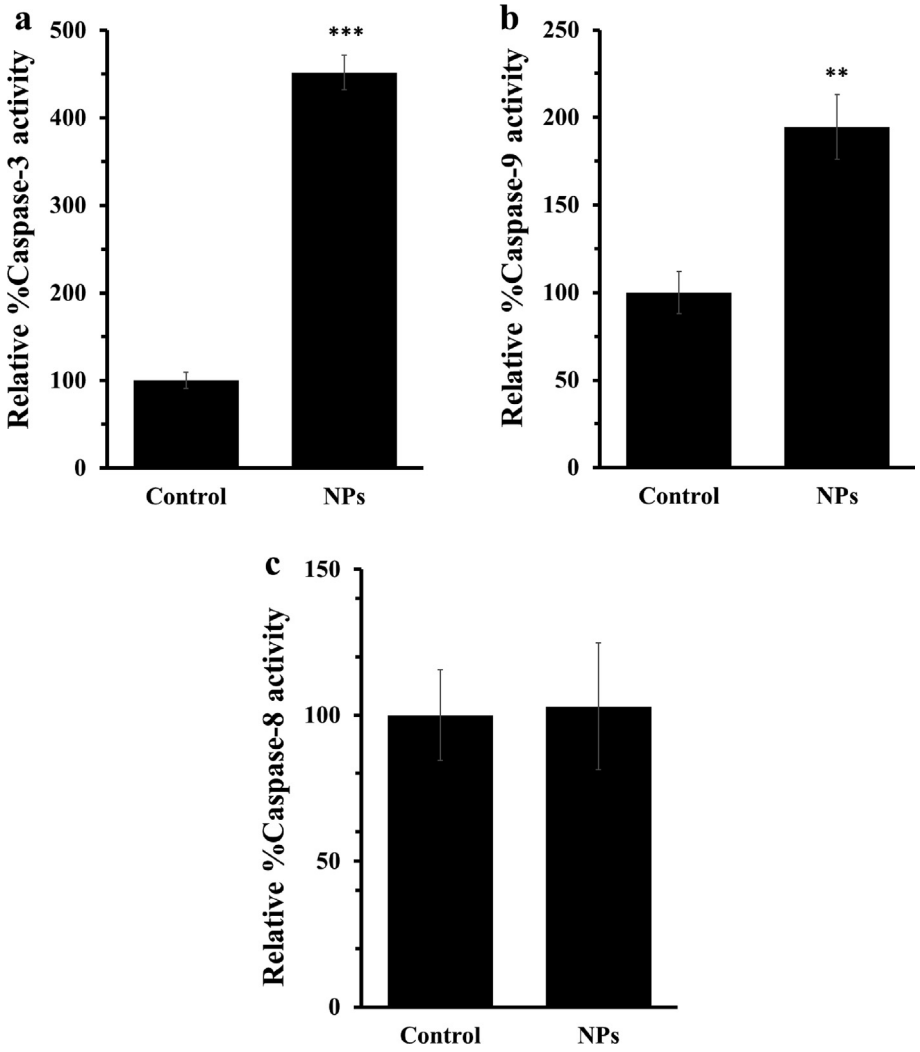

Fig. 4 (a) Caspase-3 assay, (b) caspase-9 assay, and (c) caspase-3 assay after incubation of AGS cells with IC_{50} concentrations of ZnO NPs for 24 h. Each data reported as the mean ± SD of three experiments. **p < 0.01, ***p < 0.001.

strated in Fig. 4, ZnO NPs significantly increased the activity of caspase-3 (Fig. 4a) and caspase-9 (Fig. 4b), whereas no significant changes were observed in the activity of caspase-8 (Fig. 4c). These data suggest that ZnO NPs stimulated intrinsic-mediated apoptosis in AGS cells.

3.9. Analysis of mitochondrial membrane potential

The potentiality of mitochondrial membrane serves as an important indicator of apoptosis stimulated by NPs (Yu et al., 2013). Therefore, we assessed the MMP of AGS cells after 24 h incubation with IC_{50} concentration of ZnO NPs. The data analysis indicated the loss of MMP upon exposure of AGS cells to ZnO NPs (Fig. 5). Indeed, loss of MMP in AGS cells through depolarization and dysfunction stimulated by ZnO NPs may be a main factor in triggering cell death. The overall data proved that ZnO NPs may regulate the intrinsic apoptosis signaling pathway in AGS cells.

3.10. Influence of ZnO NPs on apoptotic gene and protein expression

It was revealed that ZnO NPs may trigger cytotoxicity in AGS cells through activation of mitochondria-dependent apoptotic cell death. To further explore this effect, quantitative real-time PCR and western blot assays were conducted. In fact, expression of both anti-apoptotic and apoptotic mediators at both mRNA and protein levels upon exposure of AGS cells with IC_{50} concentration of ZnO NPs was explored by quantitative real time PCR and western blot analyses. After 24 h, the expression of apoptotic mRNA (Bax, p53, caspase-8, caspase-9, caspase-3) and anti-apoptotic mRNA (Bcl-2) as well as apoptotic and anti-apoptotic proteins (p53, Bax, Bcl-2, cytochrome *c*, caspase-9, caspase-8 and caspase-3) were quantified. It was displayed that ZnO NPs significantly suppressed the Bcl-2 expression while increased the expression of Bax, p53, caspase-8, caspase-9, and caspase-3 at both mRNA (Fig. 6a) and protein (Fig. 6b) levels when compared with control cells. It has been suggested that the increased expression level of Bax is the crucial player of the intrinsic pathway liable for the stimulation of mitochondrial dysfunction (Cory and Adams 2005, Heimer et al., 2019). The decreased level of Bcl-2 also indicated that ZnO NPs potentially mediated the induction of intrinsic apoptotic activity by suppressing the anti-apoptotic gene expression (Gibson and Davids 2015).

The current study also showed the up-regulation of p53 in the incubated AGS cells (Fig. 6a, b). From this data, the present examination proved that the up-regulation of the p53 serves as a key role in the up-regulation of the apoptosis process. It has been reported in the literature that p53 simulates apoptosis mediated by caspase activation via mitochondrial cytochrome *c* release (Gao et al., 2001, Lim et al., 2021).

Also, no significant changes were observed in the case of caspase-8 at mRNA and protein level. From this data, it is indicated that the up-regulation of p53, Bax/Bcl-2, cytochrome *c* and caspase 9 stimulated the high level of caspase 3 expression and activation.

ZnO NPs have demonstrated potential anticancer activity against a wide range of cancer cells (Bisht and Rayamajhi 2016, Anjum et al., 2021). However, most of the reported literature fail to assess the expression of genes and proteins involved in the regulation of the apoptotic pathway mediated by ZnO NPs. Hence, this study is mainly aimed to reveal the molecular mechanism of mitochondrial-mediated apoptosis pathway in AGS cells by synthesized ZnO NPs. Herein, a wide range of cellular and molecular assays were used to reveal the potential enhancement in the generation of ROS, induction of apoptosis, deactivation of antioxidant enzymes, activation of caspase-9/-3, and MMP disruption upon exposure of AGS cells to ZnO NPs. Furthermore, ZnO NPs increased the

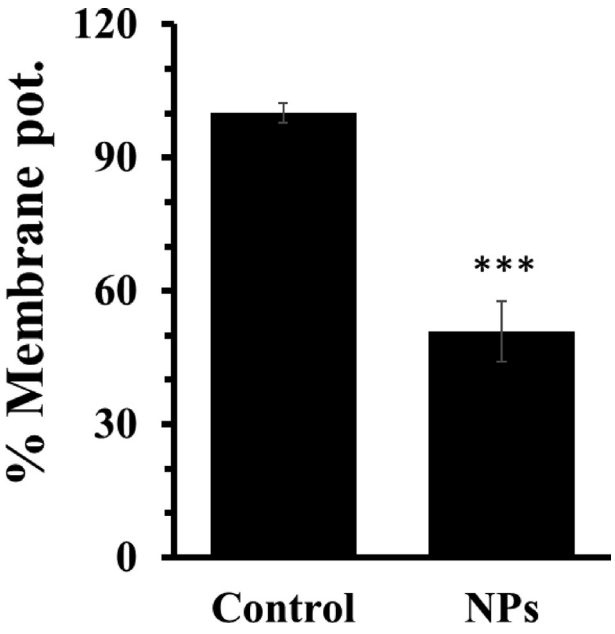

Fig. 5 Analysis of MMP after incubation of AGS cells with IC_{50} concentrations of ZnO NPs for 24 h. Each data reported as the mean ± SD of three experiments. ***p < 0.001.

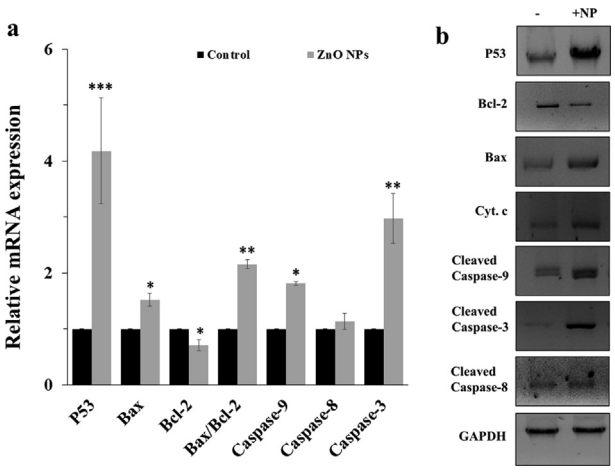

Fig. 6 (a) mRNA expression assay and (b) protein expression assay after incubation of AGS cells with IC_{50} concentrations of ZnO NPs for 24 h as determined by quantitative real time PCR and western blot analyses, respectively. Each data reported as the mean ± SD of three experiments. *p < 0.05, **p < 0.01, ***p < 0.001.

expression of P53, cytochrome *c*, caspase-9, and caspase-3, Bax/Bcl-2 ratio. This study proposes that fabricated ZnO NPs through flame spray pyrolysis approach technique can trigger selective anticancer activity against AGS cells through intrinsic apoptosis signaling pathway. In agreement with our study, it has been shown that bio-synthesized ZnO NPs were able to triggered the apoptosis in AGS cells confirmed by elevation in the sub-G1 population and overexpression of PARP at protein level (Tang et al., 2020). The extrinsic apoptotic pathway is induced by binding of transmembrane death receptors and their associated ligands, which leads to the up-regulation of caspase-8 (Gonzalvez et al., 2012, Hughes et al., 2023). The intrinsic apoptosis signaling pathway is mediated through non-receptor-associated ligands that stimulate mitochondrial mediated pathways, which cause the induction of mitochondrial disruption, loss of MMP, and release of pro-apoptotic mediators such as cytochrome *c* and Bcl-2 family proteins. Moreover, release of cytochrome *c* results in the modulation of caspase-9 and the corresponding activation of caspase-3 and apoptosis (Lossi 2022). Our data demonstrated ZnO NPs-triggered apoptosis was associated with the caspase cascade, the upregulation of p53 and Bax and down-expression of Bcl-2 and loss of MMP, indicated that ZnO NPs synthesized through flame spray pyrolysis triggered mitochondrial dysfunction and associated intrinsic apoptosis signaling pathways in gastric cancer cells.

4. Conclusion

Our study shows that the synthesized ZnO NPs through flame spray pyrolysis with a UV–visible peak around 350 nm, average size of 70 nm, hydrodynamic radius of 92.89 nm, and zeta potential of −43.13 mV mitigated AGS cell proliferation through induction of ROS production and apoptosis as confirmed by an increase in the DCF intensity and number of positive Annexin-V FITC cells, respectively. Furthermore, ZnO NPs-induced apoptosis was found to be associated with deactivation of SOD and CAT, activations of caspase-9/-3 and mitochondrial dysfunction via increases in the levels of p53, Bax, and cytochrome *c*. These findings suggest that synthesized ZnO NPs through flame spray pyrolysis approach can be considered as potential platforms for the treatment of human gastric adenocarcinoma. However, these data should be further supported by *in vivo* studies in the future.

Declaration of Competing Interest

The authors declare that they have no known competing financial interests or personal relationships that could have appeared to influence the work reported in this paper.

References

Akhtar, M.J., Ahamed, M., Kumar, S., Khan, M.M., Ahmad, J., Alrokayan, S.A., 2012. Zinc oxide nanoparticles selectively induce apoptosis in human cancer cells through reactive oxygen species. Int. J. Nanomed., 845–857

Alarifi, S., Ali, D., Alkahtani, S., Verma, A., Ahamed, M., Ahmed, M., Alhadlaq, H.A., 2013. Induction of oxidative stress, DNA damage, and apoptosis in a malignant human skin melanoma cell line after exposure to zinc oxide nanoparticles. Int. J. Nanomed., 983–993

Alavi, M., Yarani, R., 2023. ROS and RNS modulation: the main antimicrobial, anticancer, antidiabetic, and antineurodegenerative mechanisms of metal or metal oxide nanoparticles. Nano Micro Biosyst. 2 (1), 22–30.

Al-Nassar, S.I., Hussein, F.I., 2019. The effect of laser pulse energy on ZnO nanoparticles formation by liquid phase pulsed laser ablation. J. Mater. Res. Technol. 8 (5), 4026–4031.

Anjum, S., Hashim, M., Malik, S.A., Khan, M., Lorenzo, J.M., Abbasi, B.H., Hano, C., 2021. Recent advances in zinc oxide nanoparticles (ZnO NPs) for cancer diagnosis, target drug delivery, and treatment. Cancers 13 (18), 4570.

Avgustinovich, A.V., Bakina, O.V., Afanas'ev, S.G., Cheremisina, O. V., Spirina, L.V., Dobrodeev, A.Y., Buldakov, M., Choynzonov, E.L., 2021. Nanoparticles in gastric cancer management. Curr. Pharm. Des. 27 (21), 2436–2444.

Baruah, S., Dutta, J., 2009. Hydrothermal growth of ZnO nanostructures. Sci. Technol. Adv. Mater.

Bisht, G., Rayamajhi, S., 2016. ZnO nanoparticles: a promising anticancer agent. Nanobiomedicine 3 (Godište 2016), 3–9.

Carroz, J., Odencrantz, F., Finnegan, W., Drehmel, D., 1980. Aerosol generation to simulate specific industrial fine particle effluents. Am. Ind. Hyg. Assoc. J. 41 (2), 77–84.

Cory, S., Adams, J.M., 2005. Killing cancer cells by flipping the Bcl-2/Bax switch. Cancer Cell 8 (1), 5–6.

Darvishi, E., Kahrizi, D., Arkan, E., 2019. Comparison of different properties of zinc oxide nanoparticles synthesized by the green (using Juglans regia L. leaf extract) and chemical methods. J. Mol. Liq. 286, 110831.

Das, K., Samanta, L., Chainy, G.B.N., 2000. A modified spectrophotometric assay of superoxide dismutase using nitrite formation by superoxide radicals.

Das, C.A., Kumar, V.G., Dhas, T.S., Karthick, V., Kumar, C.V., 2023. Nanomaterials in anticancer applications and their mechanism of action-A review. Nanomed. Nanotechnol. Biol. Med. 47, 102613.

Debela, D.T., Muzazu, S.G., Heraro, K.D., Ndalama, M.T., Mesele, B.W., Haile, D.C., Kitui, S.K., Manyazewal, T., 2021. New approaches and procedures for cancer treatment: current perspectives. SAGE Open Med. 9, 20503121211034366.

Gao, C.F., Ren, S., Zhang, L., Nakajima, T., Ichinose, S., Hara, T., Koike, K., Tsuchida, N., 2001. Caspase-dependent cytosolic release of cytochrome c and membrane translocation of Bax in p53-induced apoptosis. Exp. Cell Res. 265 (1), 145–151.

Gibson, C.J., Davids, M.S., 2015. BCL-2 antagonism to target the intrinsic mitochondrial pathway of apoptosis. Clin. Cancer Res. 21 (22), 5021–5029.

Gonzalvez, F., Lawrence, D., Yang, B., Yee, S., Pitti, R., Marsters, S., Pham, V.C., Stephan, J.-P., Lill, J., Ashkenazi, A., 2012. TRAF2 Sets a threshold for extrinsic apoptosis by tagging caspase-8 with a ubiquitin shutoff timer. Mol. Cell 48 (6), 888–899.

Gunderson, L.L., Hoskins, R.B., Cohen, A.C., Kaufman, S., Wood, W.C., Carey, R.W., 1983. Combined modality treatment of gastric cancer. Int. J. Radiat. Oncol.* Biol.* Phys. 9 (7), 965–975.

Hameed, S., Iqbal, J., Ali, M., Khalil, A.T., Abbasi, B.A., Numan, M., Shinwari, Z.K., 2019. Green synthesis of zinc nanoparticles through plant extracts: establishing a novel era in cancer theranostics. Mater. Res. Express 6, (10) 102005.

Hasanpoor, M., Aliofkhazraei, M., Delavari, H., 2015. Microwave-assisted synthesis of zinc oxide nanoparticles. Procedia Mater. Sci. 11, 320–325.

Hasnidawani, J., Azlina, H., Norita, H., Bonnia, N., Ratim, S., Ali, E., 2016. Synthesis of ZnO nanostructures using sol-gel method. Procedia Chem. 19, 211–216.

Heimer, S., Knoll, G., Schulze-Osthoff, K., Ehrenschwender, M., 2019. Raptinal bypasses BAX, BAK, and BOK for mitochondrial outer membrane permeabilization and intrinsic apoptosis. Cell Death Dis. 10 (8), 556.

Hongmei, Z., 2012. Extrinsic and intrinsic apoptosis signal pathway review. Apoptosis and medicine. InTechOpen.

Hughes, S.A., Lin, M., Weir, A., Huang, B., Xiong, L., Chua, N.K., Pang, J., Santavanond, J.P., Tixeira, R., Doerflinger, M., 2023. Caspase-8-driven apoptotic and pyroptotic crosstalk causes cell death and IL-1β release in X-linked inhibitor of apoptosis (XIAP) deficiency. EMBO J. 42 (5), e110468.

Ilson, D.H., 2019. Advances in the treatment of gastric cancer: 2019. Curr. Opin. Gastroenterol. 35 (6), 551–554.

Jensen, J.R., Johannessen, T., Wedel, S., Livbjerg, H., 2000. Preparation of ZnO–Al_2O_3 particles in a premixed flame. J. Nanopart. Res. 2, 363–373.

Ji, F., Tian, X., Liu, X., Fu, L., Wu, Y., Fang, X., Jin, H., 2015. Dihydromyricetin induces cell apoptosis via a p53-related pathway in AGS human gastric cancer cells. Genet. Mol. Res. 14 (4), 15564–15571.

Joharatnam-Hogan, N., Shiu, K.K., Khan, K., 2020. Challenges in the treatment of gastric cancer in the older patient. Cancer Treat. Rev. 85, 101980.

Kielkopf, C.L., Bauer, W., Urbatsch, I.L., 2020. Bradford assay for determining protein concentration. Cold Spring Harbor Protocols 2020 (4) (pdb.prot102269).

Kumar, S.S., Venkateswarlu, P., Rao, V.R., Rao, G.N., 2013. Synthesis, characterization and optical properties of zinc oxide nanoparticles. Int. Nano Lett. 3, 1–6.

Li, Y., Jiang, C., Zhang, X., Liao, Z., Chen, L., Li, S., Tang, S., Fan, Z., Zhang, Q., 2022. Inhibition of ABCC9 by zinc oxide nanoparticles induces ferroptosis and inhibits progression, attenuates doxorubicin resistance in breast cancer. Cancer Nanotechnol. 13 (1), 3.

Li, B., Wang, L., Chi, B., 2013. Upregulation of periostin prevents P53-mediated apoptosis in SGC-7901 gastric cancer cells. Mol. Biol. Rep. 40, 1677–1683.

Lim, Y., Dorstyn, L., Kumar, S., 2021. The p53-caspase-2 axis in the cell cycle and DNA damage response. Exp. Mol. Med. 53 (4), 517–527.

Lossi, L., 2022. The concept of intrinsic versus extrinsic apoptosis. Biochem. J 479 (3), 357–384.

Madhumitha, G., Elango, G., Roopan, S.M., 2016. Biotechnological aspects of ZnO nanoparticles: overview on synthesis and its applications. Appl. Microbiol. Biotechnol. 100, 571–581.

Mädler, L., Kammler, H.K., Mueller, R., Pratsinis, S.E., 2002. Controlled synthesis of nanostructured particles by flame spray pyrolysis. J. Aerosol Sci. 33 (2), 369–389.

Majeed, S., Danish, M., Ismail, M.H.B., Ansari, M.T., Ibrahim, M.N. M., 2019. Anticancer and apoptotic activity of biologically synthesized zinc oxide nanoparticles against human colon cancer HCT-116 cell line-in vitro study. Sustain. Chem. Pharm. 14, 100179.

Matsoukas, T., Friedlander, S.K., 1991. Dynamics of aerosol agglomerate formation. J. Colloid Interface Sci. 146 (2), 495–506.

McCarthy, J.F., Yurek, G.J., Elliott, J.F., Amdur, M.O., 1982. Generation and characterization of submicron aerosols of zinc oxide. Am. Ind. Hyg. Assoc. J. 43 (12), 880–886.

Mohammadi Shivyari, A., Tafvizi, F., Noorbazargan, H., 2022. Anticancer effects of biosynthesized zinc oxide nanoparticles using Artemisia scoparia in Huh-7 liver cancer cells. Inorganic Nano-Metal Chem. 52 (3), 375–386.

Nagar, V., Singh, T., Tiwari, Y., Aseri, V., Pandit, P.P., Chopade, R. L., Pandey, K., Lodha, P., Awasthi, G., 2022. ZnO nanoparticles: exposure, toxicity mechanism and assessment. Mater. Today Proc.

Nagaraju, G.P., Srivani, G., Dariya, B., Chalikonda, G., Farran, B., Behera, S.K., Alam, A., Kamal, M.A., 2021. Nanoparticles guided drug delivery and imaging in gastric cancer. In: Seminars in Cancer Biology, Elsevier.

Nunes, D., Pimentel, A., Santos, L., Barquinha, P., Pereira, L., Fortunato, E., Martins, R., 2019. Synthesis, design, and morphology of metal oxide nanostructures. Metal Oxide Nanostruct., 21–57

Orditura, M., Galizia, G., Sforza, V., Gambardella, V., Fabozzi, A., Laterza, M.M., Andreozzi, F., Ventriglia, J., Savastano, B., Mabilia, . Treatment of gastric cancer. World J. Gastroenterol.: WJG 20 (7), 1635.

Parveen, K., Banse, V., Ledwani, L., 2016. Green synthesis of nanoparticles: Their advantages and disadvantages. In: AIP conference proceedings, AIP Publishing LLC.

Radziejewska, I., Supruniuk, K., Bielawska, A., 2021. Anti-cancer effect of combined action of anti-MUC1 and rosmarinic acid in AGS gastric cancer cells. Eur. J. Pharmacol. 902, 174119.

Rajeshkumar, S., Kumar, S.V., Ramaiah, A., Agarwal, H., Lakshmi, T., Roopan, S.M., 2018. Biosynthesis of zinc oxide nanoparticles usingMangifera indica leaves and evaluation of their antioxidant and cytotoxic properties in lung cancer (A549) cells. Enzyme Microb. Technol. 117, 91–95.

Ranjithkumar, B., Ramalingam, H.B., Kumar, E.R., Srinivas, C., Magesh, G., Rahale, C.S., El-Metwaly, N.M., Shekar, B.C., 2021. Natural fuels (Honey and Cow urine) assisted combustion synthesis of zinc oxide nanoparticles for antimicrobial activities. Ceram. Int. 47 (10), 14475–14481.

Redza-Dutordoir, M., Averill-Bates, D.A., 2016. Activation of apoptosis signalling pathways by reactive oxygen species. Biochimica et Biophysica Acta (BBA)-Molecular Cell Res. 1863 (12), 2977–2992.

Shamasi, Z., Es-haghi, A., Taghavizadeh Yazdi, M.E., Amiri, M.S., Homayouni-Tabrizi, M., 2021. Role of Rubia tinctorum in the synthesis of zinc oxide nanoparticles and apoptosis induction in breast cancer cell line. Nanomed. J. 8 (1), 65–72.

Shanmugam, K., Sellappan, S., Alahmadi, T.A., Almoallim, H.S., Natarajan, N., Veeraraghavan, V.P., 2022. Green synthesized zinc oxide nanoparticles from Cinnamomum verum bark extract inhibited cell growth and induced caspase-mediated apoptosis in oral cancer KB cells. J. Drug Delivery Sci. Technol. 74, 103577.

Siddiqi, A., Johnston, F.M., 2023. The perioperative and operative management of esophageal and gastric cancer. Surg. Oncol. Clin. 32 (1), 65–81.

Sinha, A.K., 1972. Colorimetric assay of catalase. Anal. Biochem. 47 (2), 389–394.

Strobel, R., Baiker, A., Pratsinis, S.E., 2006. Aerosol flame synthesis of catalysts. Adv. Powder Technol. 17 (5), 457–480.

Sujitha, M.V., Kannan, S., 2013. Green synthesis of gold nanoparticles using Citrus fruits (Citrus limon, Citrus reticulata and Citrus sinensis) aqueous extract and its characterization. Spectrochim. Acta A Mol. Biomol. Spectrosc. 102, 15–23.

Tang, Q., Xia, H., Liang, W., Huo, X., Wei, X., 2020. Synthesis and characterization of zinc oxide nanoparticles from Morus nigra and its anticancer activity of AGS gastric cancer cells. J. Photochem. Photobiol. B Biol. 202, 111698.

Tani, T., Mädler, L., Pratsinis, S.E., 2002. Homogeneous ZnO nanoparticles by flame spray pyrolysis. J. Nanopart. Res. 4 (4), 337–343.

Teimouri, M., Khosravi-Nejad, F., Attar, F., Saboury, A.A., Kostova, I., Benelli, G., Falahati, M., 2018. Gold nanoparticles fabrication by plant extracts: synthesis, characterization, degradation of 4-nitrophenol from industrial wastewater, and insecticidal activity–a review. J. Clean. Prod. 184, 740–753.

Trommer, R., Alves, A., Bergmann, C., 2010. Synthesis, characterization and photocatalytic property of flame sprayed zinc oxide nanoparticles. J. Alloy. Compd. 491 (1–2), 296–300.

Ulrich, G.D., 1971. Theory of particle formation and growth in oxide synthesis flames. Combust. Sci. Technol. 4 (1), 47–57.

Villanueva, Y.Y., Liu, D.-R., Cheng, P.T., 2006. Pulsed laser deposition of zinc oxide. Thin Solid Films 501 (1–2), 366–369.

Vinayagam, R., Pai, S., Varadavenkatesan, T., Pugazhendhi, A., Selvaraj, R., 2021. Characterization and photocatalytic activity of ZnO nanoflowers synthesized using Bridelia retusa leaf extract. Appl. Nanosci., 1–10

Vinayagam, R., Sharma, G., Murugesan, G., Pai, S., Gupta, D., Narasimhan, M.K., Kaviyarasu, K., Varadavenkatesan, T., Selvaraj, R., 2022. Rapid photocatalytic degradation of 2, 4-dichlorophenoxy acetic acid by ZnO nanoparticles synthesized

using the leaf extract of Muntingia calabura. J. Mol. Struct. 1263, 133127.

Vinayagam, R., Pai, S., Murugesan, G., Varadavenkatesan, T., Selvaraj, R., 2023. Synthesis of photocatalytic zinc oxide nanoflowers using Peltophorum pterocarpum pod extract and their characterization. Appl. Nanosci. 13 (1), 847–857.

Wang, C., Hu, X., Gao, Y., Ji, Y., 2015. ZnO nanoparticles treatment induces apoptosis by increasing intracellular ROS levels in LTEP-a-2 cells. BioMed Res. Int. 2015.

Wiesmann, N., Tremel, W., Brieger, J., 2020. Zinc oxide nanoparticles for therapeutic purposes in cancer medicine. J. Mater. Chem. B 8 (23), 4973–4989.

Yang, L., 2006. Incidence and mortality of gastric cancer in China. World J. Gastroenterol. 12 (1).

Yang, L., Ying, X., Liu, S., Lyu, G., Xu, Z., Zhang, X., Li, H., Li, Q., Wang, N., Ji, J., 2020. Gastric cancer: Epidemiology, risk factors and prevention strategies. Chin. J. Cancer Res. 32 (6), 695.

Yu, K.-N., Yoon, T.-J., Minai-Tehrani, A., Kim, J.-E., Park, S.J., Jeong, M.S., Ha, S.-W., Lee, J.-K., Kim, J.S., Cho, M.-H., 2013. Zinc oxide nanoparticle induced autophagic cell death and mitochondrial damage via reactive oxygen species generation. Toxicol. in Vitro 27 (4), 1187–1195.

Zein, R., Sharrouf, W., Selting, K., 2020. Physical properties of nanoparticles that result in improved cancer targeting. J. Oncol.